

# Anodization of Ti6Al4V in Water-Ethylene Glycol Solution Containing NH<sub>4</sub>F and Its Corrosion Behavior in Ringer's Solution

Irem Cemre Turu\* and Nurhan Cansever

Yildiz Technical University, Faculty of Chemistry-Metallurgy, Metallurgical and Materials Engineering Department, 34210 Esenler, Istanbul-Turkey

\*E-mail: [туру@yildiz.edu.tr](mailto:туру@yildiz.edu.tr)

Received: 8 February 2022 / Accepted: 25 March 2022 / Published: 7 May 2022

---

In this study, Ti6Al4V samples were anodized at room temperature with a constant voltage of 30 V for 3 hours in ethylene glycol solutions containing 0.25% NH<sub>4</sub>F by weight and 2.5%, 5% and 10% deionized H<sub>2</sub>O by volume. After the anodization, the structure and crystallinity of the oxide layers were investigated by Field-Emission Scanning Electron Microscopy and X-ray diffraction methods, respectively. According to the findings, all anodized samples exhibited crystalline TiO<sub>2</sub> nanotubular structures composed of rutile and anatase. FESEM analyzes showed that the thickness of the nanotube layer decreased accordingly with increasing H<sub>2</sub>O content in the organic anodizing medium. For comparison, electrochemical behaviors of the anodized and untreated Ti6Al4V samples were evaluated in Ringer's solution at 37 °C by electrochemical impedance spectroscopy and potentiodynamic polarization techniques. According to the results, the anodized samples which had nanotubular structures, exhibited better corrosion behavior than untreated Ti6Al4V. Furthermore, electrochemical analyses also revealed that increase of H<sub>2</sub>O content in ethylene glycol lowered the corrosion resistance of the anodized samples by affecting the morphology, structure and the length of the nanotubes.

---

**Keywords:** Ti6Al4V, TiO<sub>2</sub> nanotubes, Impedance Spectroscopy, Ringer's solution.

## 1. INTRODUCTION

The effect of surface modification on Ti and its alloys have been extensively studied for biomedical applications. It has been reported that surface modification techniques enhanced properties such as increased surface area and roughness, promoting better cell adhesion, and in many cases, increasing the biocompatibility of the material for use as an implant [1,2]. As a valve metal, Ti has an oxide layer on its surface that provides corrosion resistance [3]. However, the corrosion properties of

this metal can be further improved by changing the type and structure of the oxide layer. Particularly, nanotubes and nanoporous oxides are known to have much better corrosion properties than the barrier type  $\text{TiO}_2$  [4]. Therefore, formation of  $\text{TiO}_2$  nanotubes on implant materials has received great attention due to their better biocompatibility, especially for bioapplications. A few of these biocompatibility benefits are improvement of osteoblast growth and differentiation into osteocytes, promoting cell adhesion for better bone formation, and enhanced tissue integration [5–8].

Anodic oxidation has been an approved and well-studied method to produce  $\text{TiO}_2$  nanotubes on Ti and its alloys [9–11].  $\text{TiO}_2$  nanostructures with different physical properties such as pore size and morphology can be controlled by anodizing parameters such as anodization time, potential and electrolyte composition. These parameters are known to have important effects on oxide growth and dissolution rates, which are the key parameters affecting nanotube formation [5,8,12–14].

As  $\text{F}^-$  ions play a major role in nanotubular oxide growth, electrolytes containing  $\text{F}^-$  ions are specifically preferred for successful nanotube growth [15–18]. In nanotubular oxide growth, the formation and dissolution of the oxide layer occur simultaneously on the Ti surface. In this process,  $\text{F}^-$  ions are the key components due to their high chemical affinity for Ti and high diffusibility because of their small atomic radii. Thus, during the oxidation process, formation of the compact  $\text{TiO}_2$  layer and dissolution of this layer to form water-soluble  $[\text{TiF}_6]^{2-}$  occurs simultaneously. Consequently, as a diffusion-driven process, with sufficient time and electrical field, nanotubes may form on Ti or alloy substrate [19]. Additionally, the pH of the anodization medium and the source of  $\text{F}^-$  ions are also important. In the literature,  $\text{TiO}_2$  nanotube formation has been successfully performed using acidic, aqueous or organic electrolytes containing  $\text{F}^-$  ions [4,8,15,18]. Electrolytes containing  $(\text{NH}_4)_2\text{SO}_4$  and  $\text{NH}_4\text{F}$  [5]; ethylene glycol,  $\text{NH}_4\text{F}$  and  $\text{H}_2\text{O}$  [20];  $\text{H}_3\text{PO}_4$  and  $\text{HF}$  [17];  $\text{HF}$  and  $\text{H}_2\text{O}$  [21] have also been reported for the anodic oxidation of  $\text{TiO}_2$  nanotubes on Ti6Al4V alloy.

Besides  $\text{F}^-$  ions, it has been reported that  $\text{H}_2\text{O}$  content in organic electrolytes has a significant effect on  $\text{TiO}_2$  nanotube morphology and crystal structure [9,22–24]. Change in pore diameter and nanotube length with varying  $\text{H}_2\text{O}$  content in EG electrolyte has also been noted [8,23]. In addition, Su et al. obtained  $\text{TiO}_2$  nanotubes with different crystal structures by changing the amount of  $\text{H}_2\text{O}$  in EG-based anodization solution [24].

In this study, Ti6Al4V substrate was chosen as it provides better biocompatibility with its elastic modulus similar to that of human bone. Nanotubular oxide growth was carried out by anodic oxidation in EG electrolytes containing 0.25%  $\text{NH}_4\text{F}$  by weight and 2.5%, 5% and 10%  $\text{H}_2\text{O}$  by volume. The effect of  $\text{H}_2\text{O}$  content on structural and electrochemical properties of  $\text{TiO}_2$  nanotubes was investigated. Field-Emission Scanning Electron Microscopy (FESEM) was used for observing surface morphology of the  $\text{TiO}_2$  nanotubes on Ti6Al4V substrate. Crystal phases of the anodized Ti6Al4V as well as the untreated Ti6Al4V was investigated using the X-ray diffraction (XRD) method. Since the chemical interaction between metallic materials and human body was crucial for evaluating the stability and overall performance of an implant material, the electrochemical corrosion behavior of anodized samples was evaluated and compared with untreated Ti6Al4V sample using electrochemical impedance spectroscopy (EIS) and potentiodynamic polarization technique in Ringer's solution.

## 2. EXPERIMENTAL

In order to observe the effect of H<sub>2</sub>O content on TiO<sub>2</sub> nanotube structures in the anodization medium, TiO<sub>2</sub> nanotubes were grown on Ti6Al4V substrate consisting of 89.13% Ti, 6.36% Al, 4.14% V, 0.21% Fe and 0.11% other elements. The samples with dimensions of 10 mm × 10 mm × 2 mm were cut, prepared metallographically using 240 and 320 grit SiC papers, and then polished with 9 μm diamond paste and 0.04 μm colloidal silica. Afterward, the samples were cleaned in an ultrasonic bath with ethanol and deionized water and dried in the air before anodic oxidation.

The anodization was performed using a direct current power supply with a two-electrode setup, in which the sample was attached as the anode and a 2.5 cm × 4.0 cm graphite plate was used as the cathode. In order to provide a homogeneous electric field distribution in the electrolyte, the distance between anode and cathode was kept constant at 2 cm in all anodizing processes. Using this setup, each sample was anodized in EG solution for 3 hours at a constant voltage of 30 V at room temperature, and current-time data were recorded for each process. To observe the effect of H<sub>2</sub>O content on different properties of TiO<sub>2</sub> nanotubes, EG electrolytes containing 0.25 % NH<sub>4</sub>F by weight were prepared with three different percentages of deionized H<sub>2</sub>O as 2.5%, 5% and 10% by volume. The electrolyte was stirred continuously at 300 rpm during all the anodization processes. After anodic oxidation, the samples were rinsed with distilled water, ultrasonically cleaned with propanol, and dried in the air.

The surface morphology of the anodized samples was examined using a Philips-FEI XL30 FESEM. In order to observe the crystal structure of TiO<sub>2</sub> nanotubes, low grazing angle XRD analyzes (PANalytical X'Pert PRO) were performed on samples with 1° incidence angle using Cu-Kα radiation.

To observe the biocompatibility of the samples and to simulate the conditions in human body as close as possible, all electrochemical analysis were carried out in Ringer's solution at 37°C (8.6 g NaCl, 0.33 g CaCl<sub>2</sub>·2H<sub>2</sub>O, 0.3 g KCl in 1l of deionized water) which had similar ionic properties to that of human body fluid. Electrochemical behavior of TiO<sub>2</sub> nanotubes was investigated by using potentiodynamic polarization and EIS analyzes. Before each electrochemical test, to observe the stability of samples and to ensure similar surface conditions in Ringer's solution, samples were kept in the solution for approximately 10 minutes and the open circuit potential was recorded. After that, to observe the potentiodynamic response of TiO<sub>2</sub> nanotubes in Ringer's solution, each sample was scanned from 150 mV below the observed open circuit potential value to 1.5 V at a scan rate of 10 mV/s. To observe the impedance response of TiO<sub>2</sub> nanotubes grown on Ti6Al4V samples, a sine signal with an amplitude of 5 mV relative to the open circuit potential was applied to the sample and the frequency range of 0.01 Hz to 10 kHz was scanned. In all electrochemical analyzes, 2 graphite electrodes were used as counter, and calomel electrode as reference electrodes.

## 3. RESULTS AND DISCUSSION

Figure 1 presented the current vs time plots of each sample that was anodized in EG solution with three different H<sub>2</sub>O contents. According to the figure, each sample presented the unique characteristic peaks of the tube formation [25].

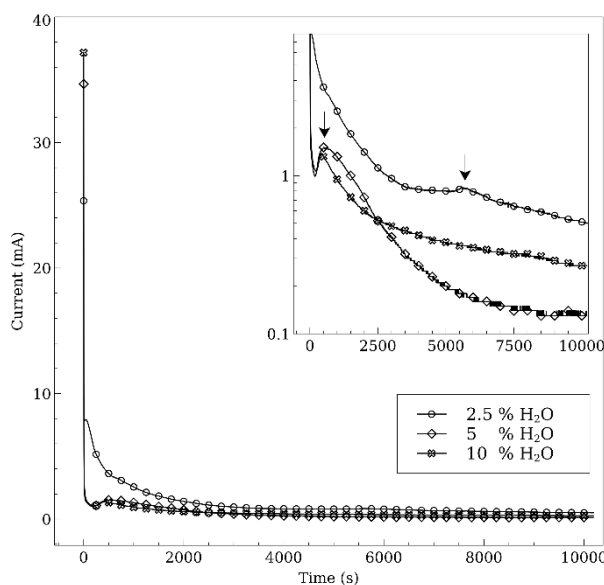


**Figure 1.** Current-time plots of Ti6Al4V samples anodized in different H<sub>2</sub>O contents in EG containing 0.25% NH<sub>4</sub>F.

Initial current value of each sample was recorded as 37.16, 34.67 and 25.36 mA for the samples anodized in the electrolytes with 10%, 5% and 2.5% H<sub>2</sub>O contents, respectively. It was observed that the initial current values were influenced by the anodization solution. It was clear that a higher H<sub>2</sub>O content resulted in occurrence of higher current values which were correlated with the viscosity of EG and the mobility of ions in the solution. In organic electrolytes such as EG, H<sub>2</sub>O acts as a diluent and increases the mobility of ions by reducing the viscosity of the solution. This phenomenon was also discussed in previous studies with similar findings specifically for aqueous organic solutions [24,26-28]. Following this initial point, the current values dropped sharply to a minimum and then slightly raised to a second maximum. The lowest point observed was 1.07 mA for 5%, 10% and 7.07 mA for 2.5% H<sub>2</sub>O contents. This decrease in current was governed by the growth of the thin, compact barrier oxide layer. After the formation of the barrier layer, F<sup>-</sup> ions attacked the previously formed barrier layer, and the release of electrons due to electrochemical processes during the dissolution of the barrier oxide caused the current values to rise again [4,29]. In addition, the reduction in oxide thickness by dissolving the oxide layer resulted in lower electrical resistance, thus allowing higher current values [30]. After the occurrence of the second peak, the current values decayed slightly and remained constant until the end of the anodization process. In fact, these stages of the current-time curves were well described in previous studies. Nevertheless, these stages contained invaluable data for the anodization and tube formation. According to Figure 1, although current-time characteristics were similar, the time when the second current peak was observed and the subsequent decay section of the curve was different for each sample. The second peak occurring at 1.45 mA for 5% H<sub>2</sub>O and 10% H<sub>2</sub>O was observed approximately fifteen minutes after the constant voltage was applied. On the other hand, the second peak was observed at 0.84 mA for 2.5% H<sub>2</sub>O and after approximately 95 minutes of voltage application. This second peak could be directly related to the pore size of the nanotubes. According to a study on Ti foil substrates, the value of the second current peak was associated with the dissolution of the barrier layer formed earlier

and the larger pores were reported as the chemical reaction increased [4,28,30]. This result also supported our findings that the average pore size was slightly lower for 2.5% H<sub>2</sub>O, which presented a lower second current peak. It should also be noted that no current fluctuations were observed in Figure 1, which was a benefit of organic anodization solution that promoted the formation of smoother tube structures. Macak et al. suggested that fluctuations in current caused the formation of irregular tube walls [31]. Moreover, the pore diameter, as well as the thinning of the tube walls, were associated with the anodizing solution. According to previous studies, when aqueous solutions and F<sup>-</sup> containing glycerol were compared, both solutions provided lower current and smaller pore diameters. However, smoother pore structures have been reported in glycerol, which obviously has a higher viscosity [31]. In another study, Suliali et al. studied with NH<sub>4</sub>F containing EG solution to grow nanotubes on Ti foil substrates. The authors observed similar findings and reported that the smallest pore diameter was observed in the 1.5 M NH<sub>4</sub>F solution. In line with our report, the authors also observed smaller and delayed peak and a smooth decay [30].

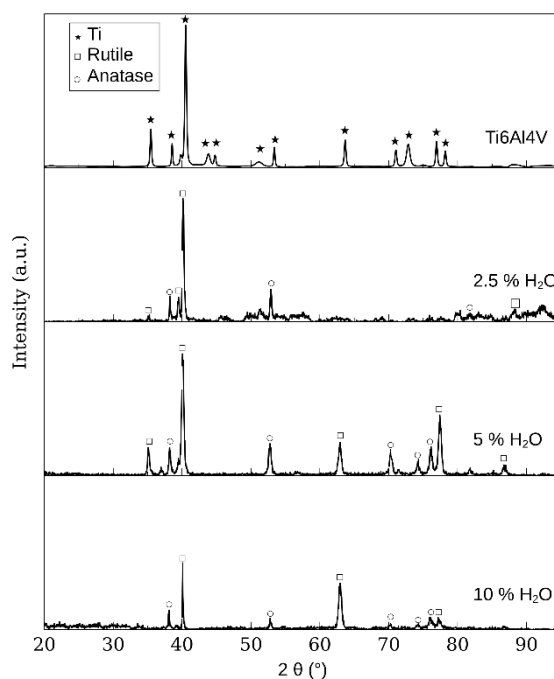


**Figure 2.** XRD patterns of untreated and anodized Ti6Al4V substrates in EG containing 0.25% NH<sub>4</sub>F and different H<sub>2</sub>O contents.

The crystal structure of anodized Ti6Al4V as well as untreated Ti6Al4V was given as Figure 2. According to XRD analyzes, all anodized samples had crystalline structure. The anodic oxidated samples exhibited some crystalline reflections corresponding to the substrate metal, as well as the mixed TiO<sub>2</sub> crystal phase of rutile [32], anatase [33] and Ti<sub>2</sub>O<sub>3</sub> [34] phases. The relation between phase transformation and H<sub>2</sub>O content as well as the anodization potential have also been discussed in the literature. It was reported that the highest change in crystal structure was observed at the highest H<sub>2</sub>O content and the highest electrical potential [23]. However, in our case, considering that the samples were grown under the same electrical potential, the change in crystal structure was only affected by the H<sub>2</sub>O content. The samples anodized in 5% and 10% H<sub>2</sub>O content exhibited slightly higher number of

reflections than the sample anodized in solution containing 2.5% H<sub>2</sub>O. The crystal structure of TiO<sub>2</sub> has been extensively investigated in the literature. In these studies, porous anodic films grown on Ti consisted of rutile and/or anatase phases, which showed a higher apatite forming ability than amorphous TiO<sub>2</sub> and therefore better biocompatibility in experiments performed in body fluids [35,36].

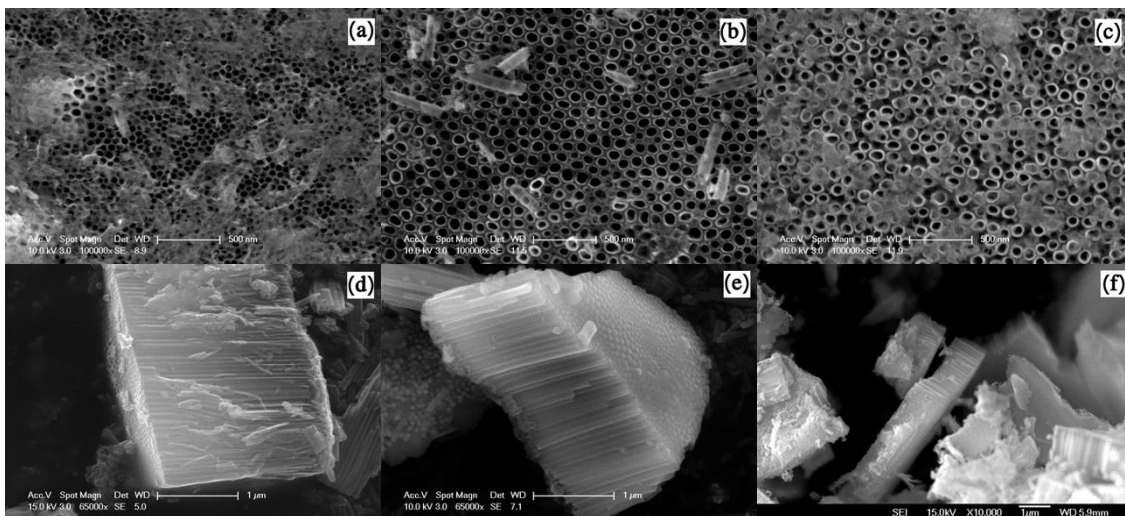


**Figure 3.** Surface and cross-sectional FESEM images of TiO<sub>2</sub> nanotubes on Ti6Al4V substrates anodized in different H<sub>2</sub>O contents: **a,d**) 2.5% H<sub>2</sub>O, **b,e**) 5% H<sub>2</sub>O and **c,f**) 10% H<sub>2</sub>O.

Surface morphology of the anodic oxidized samples and cross-sectional images of TiO<sub>2</sub> nanotubes were shown in Figure 3 a-f. According to these FESEM images, the distinctive feature of the nanotubes and the effect of H<sub>2</sub>O content on morphologies were noticeable. It was observed that nanotubes grown at 2.5% H<sub>2</sub>O had thin tube walls and ordered, hexagonal shaped pores. On the other hand, regular, rounder pores and thicker tube walls were the defining features of the samples grown at 5% H<sub>2</sub>O. In addition, the sample that was anodized in the solution containing 10% H<sub>2</sub>O, which was the highest H<sub>2</sub>O content in our experiments, had nanotubes with slightly thinner tube walls than the sample oxidized in the solution containing 5% H<sub>2</sub>O. Also, due to the dissolution of tube walls, the nanotubes were appeared to be free standing rather than being etched in a continuous oxide layer. In fact, the etching process of the oxide layer was affected not only by the presence of F<sup>-</sup> ions in the oxidizing medium, but also by the chemical composition of the substrate material. Thus, it could be said that the overall shape and the ordered structure of the tubes were controlled by both the parameters of the anodization process and the substrate. In fact, the F<sup>-</sup> ions not only affected the dissolution/etching process, but also the oxide structure itself. It was reported that H<sub>2</sub>O-soluble F<sup>-</sup> ion played the major role in tube formation [37]. Moreover, although nanotubes were mainly composed of TiO<sub>2</sub>, it was reported that the tubes contained F<sup>-</sup> ions as well as traces of alloying elements of the substrate material [38].

Pore diameters were measured as 52.5 nm, 81.3 nm and 72.9 nm for the 2.5%, 5% and 10% H<sub>2</sub>O contents, respectively. Firstly, increasing H<sub>2</sub>O content in the anodizing medium increased the dissolution of the oxides, resulting in larger pores. However, as seen in the FESEM images, the pore diameters of the nanotubes prepared in the oxidation medium with 10% H<sub>2</sub>O content decreased slightly with the formation of discrete tubes with intertubular space between them. On the other hand, nanotube length

was found to be inversely proportional to the increasing H<sub>2</sub>O content. The tube lengths corresponding to the samples prepared at 2.5%, 5% and 10% H<sub>2</sub>O contents were observed as 1584 nm, 1491 nm and 1007 nm, respectively. Since the H<sub>2</sub>O plays a role both in the formation of TiO<sub>2</sub> nanotubes and in the chemical dissolution reactions of oxides [9], this trend can be associated with the dissolution of nanotubes starting from the top due to the increased H<sub>2</sub>O content in the electrolyte. Similarly, Valota et al. observed a significant decrease in nanotube length with increasing H<sub>2</sub>O content in organic electrolyte [39]. Furthermore, Kim and Choi investigated the effect of different anodization parameters on TiO<sub>2</sub> nanotubes and reported a decrease in the thickness of the nanotubular layer with increasing H<sub>2</sub>O content in ethylene glycol solution [8]. However, contrary findings were found in the literature on the relation between nanotube length and H<sub>2</sub>O content. Liu et al. observed and reported a direct relationship between H<sub>2</sub>O content and nanotube length [26].

Anodic polarization behavior of each sample in Ringer's solution was presented in Figure 4. As can be seen in Figure 4, all the samples had similar cathodic behavior. The anodic current for Ti6Al4V started to rise up to 334  $\mu$ A at 1.32  $\mu$ A where the experiment ended. Although the oxide growth slowed down around 118  $\mu$ A, a full passivation property was not attained. Similar results were also discussed in the literature for Ti6Al4V in Ringer's solution. Pohrelyuk et al. reported that they observed a short passivation in Ringer's solution. The authors also discussed that the passivation behavior was affected by the temperature of the solution.

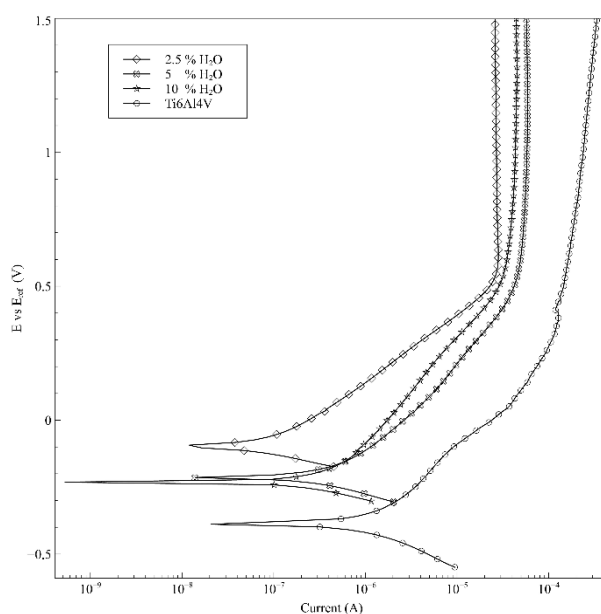


**Figure 4.** Potentiodynamic polarization plots of untreated Ti6Al4V substrate and anodized Ti6Al4V in Ringer's solution.

According to their findings, the behavior of oxide was related to the type of oxide formed on metal surface [40]. Besides solution temperature, another study showed that the anodic and passivation behavior of Ti6Al4V was also related to the microstructure of the alloy. Authors reported results similar

to our findings [41]. On the other hand, all anodized samples showed passivation behavior. For the samples prepared at 2.5% H<sub>2</sub>O content, the anodic current started to increase from 0.1  $\mu$ A to 0.2  $\mu$ A with a linear rate, and the passivation current was reached here. In addition, the anodic current started to increase around 0.4  $\mu$ A for the samples prepared at 5% H<sub>2</sub>O and 10% H<sub>2</sub>O contents, and the critical passivation current was observed at 0.2  $\mu$ A, similar to the sample prepared at 2.5% H<sub>2</sub>O. Thus, all anodized samples had passivation behavior at approximately 0.5 V to 1.5 V.

The corrosion potential ( $E_{\text{corr}}$ ) and corrosion current density ( $I_{\text{corr}}$ ) values of the samples were given in Table 1.  $E_{\text{corr}}$  values of Ti6Al4V substrate and samples prepared at 2.5%, 5% and 10% H<sub>2</sub>O contents were observed as -0.388 V, -0.093 V, -0.214 V and -0.231 V, respectively. Evidently, all anodized samples had higher  $E_{\text{corr}}$  values, a confirmation of better corrosion resistance. On the other hand, when the anodized samples were compared with each other in terms of  $E_{\text{corr}}$  values, the protective property of the oxide layer decreased with increasing H<sub>2</sub>O content in anodization solution, which affected the physical properties of TiO<sub>2</sub> nanotubes as presented in the FESEM images. As seen in Table 1, the  $E_{\text{corr}}$  values of the samples prepared at 5% H<sub>2</sub>O and 10% H<sub>2</sub>O contents were close to each other, and the highest  $E_{\text{corr}}$  value among all samples was measured as -0.093 V in the sample prepared at 2.5% H<sub>2</sub>O content. Additionally,  $I_{\text{corr}}$  values were found as 3.497, 0.078, 0.190 and 0.213  $\mu$ A/cm<sup>2</sup> for the Ti6Al4V substrate and the anodized samples prepared at 2.5%, 5% and 10% H<sub>2</sub>O contents, respectively. Both  $E_{\text{corr}}$  and  $I_{\text{corr}}$  values showed that corrosion resistance of the anodized samples was higher than the Ti6Al4V substrate, and the increasing H<sub>2</sub>O content in the anodizing medium caused a negative effect on corrosion properties of the anodized samples with TiO<sub>2</sub> nanotubes. In literature, different opinions and findings have been reported for corrosion behavior of TiO<sub>2</sub> nanotubes. Many of these studies evaluated their results according to the anodization solution, the substrate on which the nanotubes were grown, and the medium in which the electrochemical tests were performed. Sivasprakash et al. studied the formation of TiO<sub>2</sub> nanotubes on Ti substrate in NH<sub>4</sub>F containing EG solution with two different anodization voltages. According to their findings of electrochemical tests performed in simulated body fluids, corrosion resistance increased with increasing H<sub>2</sub>O content in the anodization medium [23].

**Table 1.** Corrosion related data calculated by polarization curve of untreated Ti6Al4V substrate and anodized Ti6Al4V in Ringer's solution.

Sample	$E_{\text{corr}}$ (V)	$I_{\text{corr}}$ ( $\mu$ A/cm <sup>2</sup> )
Ti6Al4V	- 0.388	3.497
2.5% H <sub>2</sub> O	- 0.093	0.078
5% H <sub>2</sub> O	- 0.214	0.190
10% H <sub>2</sub> O	- 0.231	0.213

Both anodized samples and native oxide of Ti6Al4V were analyzed using impedance spectroscopy. Impedance spectroscopy is a powerful tool for understanding the nature of a material's surface in a specific solution. By applying a sine signal with respect to a reference electrode, the

characteristic features of the surface can be observed by fitting an electrical equivalent circuit to the gathered data. In this respect, unique features of the surface associated with certain circuit elements of the equivalent circuit can then be affiliated by the observer accordingly.

According to Figure 5, all impedance data featured characteristic semicircular arcs. At first glance, Ti6Al4V and the sample anodized at 2.5% H<sub>2</sub>O content had similar behavior, while the samples prepared in 5% and 10% H<sub>2</sub>O contents had much smaller semicircular arc in the high frequency regions, followed by an increase in  $-Z_{\text{img}}$  with respect to  $Z_{\text{real}}$  in the low frequency region of the spectrum. This increase in imaginary Z in the low frequency region was attributed to rapid ionic diffusion processes and in our case this behavior was observed in the samples prepared at 5% and 10% H<sub>2</sub>O contents, which had higher pore diameter and shorter nanotube length than the sample prepared at 2.5% H<sub>2</sub>O content [42]. Moreover, all anodized samples had a significantly higher semicircular radius than Ti6Al4V indicating all anodized samples exhibited better corrosion resistance than untreated Ti6Al4V substrate. Moreover, when anodized samples were compared with each other, the semi-circle radius was observed to be smaller with increasing H<sub>2</sub>O content. This finding was also supported by anodic polarization findings.

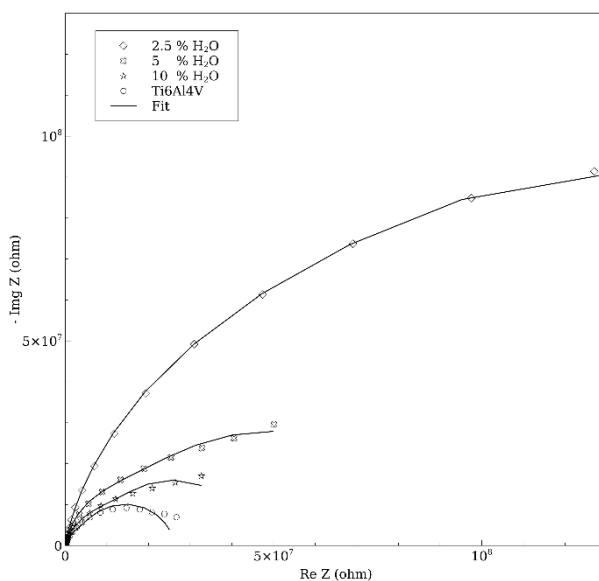


**Figure 5.** Nyquist plots of untreated Ti6Al4V substrate and anodized Ti6Al4V in Ringer's solution.

The impedance data was further analyzed for deeper investigation to identify the corrosion related characteristics of the oxide layer. For this purpose, two electrical equivalent circuits as given in Figure 6a and 6b were used for fitting the impedance data. Figure 6a, which was used for fitting to the electrochemical impedance data of Ti6Al4V, included double layer admittance ( $Y_{\text{dl}}$ ), charge transfer resistance ( $R_{\text{ct}}$ ), the admittance of oxide layer ( $Y_{\text{ox}}$ ), the resistance of oxide ( $R_{\text{ox}}$ ) and the solution resistance ( $R_{\text{sol}}$ ). Moreover, as presented as Figure 6b, the equivalent circuit that was used for fitting anodized samples, was more complex as nanotubes on Ti6Al4V surface had different physical features such as the barrier layer, nanotube walls and the pores. In order to fathom these features, parallel capacitance and resistance couples were employed. Thus  $R_{\text{pr}}$ ,  $R_{\text{w}}$  described the resistances of pore and nanotube wall, respectively. In addition,  $Y_{\text{opr}}$ ,  $Y_{\text{ow}}$  values conjured the admittance of pore and wall

structures. Then,  $C_{pr}$  and  $C_{ow}$  values were calculated using a transfer function and the  $Y_{opr}$ ,  $Y_{ow}$ ,  $n_{pr}$ ,  $n_w$  values [3,43,44]. All calculated values for impedance analyzes were summarized in Tables 2 and 3.

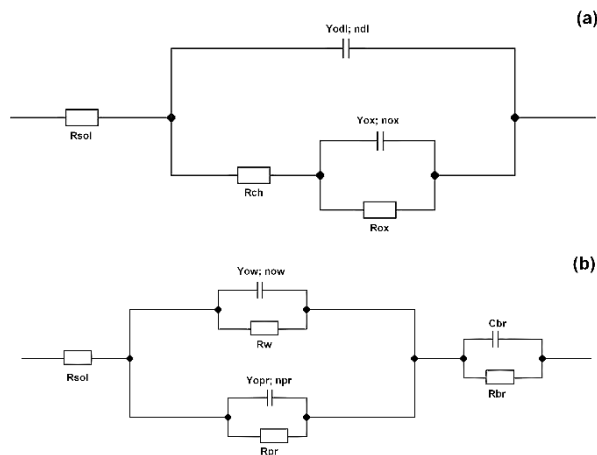


**Figure 6.** Equivalent electrical circuits used for fitting EIS data **a)** untreated Ti6Al4V, **b)** anodized Ti6Al4V.

In impedance spectroscopy, the combination of  $C_w$  and  $R_w$  values were used for evaluating the overall performance of nanotube walls in Ringer’s solution. As could be followed in Table 2,  $C_w$  values were comparable to each other with a slight variation in 5%  $H_2O$  content. Additionally, the  $R_w$  values which showed the resistivity of the tube wall decreased with increasing  $H_2O$  content in anodization solution. It was also noted that the decrease was prominent for 10%  $H_2O$ . The decrease in  $R_w$  values indicated that the protective properties of the oxide against the Ringer’s solution also decreased with increasing  $H_2O$  content. This finding was also supported by Figure 4 and Figure 5. It was shown in the Nyquist plot that the semi-circle radius was diminished with increasing  $H_2O$  content. Furthermore, in Figure 4, anodic polarization curves shifted to more negative values with increasing  $H_2O$  content in anodization solution.

**Table 2.** Equivalent electrical circuit fitting results of untreated Ti6Al4V sample.

	$R_{sol}$ (ohm)	$Y_{0ox}$ ( $S.s^n$ ) $\times 10^{-5}$	$n_{ox}$	$R_{ox}$ (ohm) $\times 10^3$	$C_{ox}$ (F) $\times 10^{-6}$	$Y_{odl}$ ( $S.s^n$ ) $\times 10^{-5}$	$n_{dl}$	$R_{ch}$ (ohm) $\times 10^3$	$C_{dl}$ (F) $\times 10^{-6}$
Ti6Al4V (native oxide)	3.05	9.73	0.9	23	160	6.0	0.9	3.36	52.3

As described earlier,  $C_{pr}$  and  $R_{pr}$  values could be used for evaluating the pore structure. As seen in Table 2 and 3,  $C_{pr}$  values of the samples prepared at 2.5%  $H_2O$  and 5%  $H_2O$  contents were similar and the values increased significantly with increasing  $H_2O$  content in the solution. Thus, this finding was related to the pore structure. According to FESEM micrographs, although the pore diameters were similar, especially for nanotubes grown at 5% and 10%  $H_2O$  content, the pore structure changed

significantly. While thin walls with hexagonal shaped pores were dominant in the samples prepared at 2.5% H<sub>2</sub>O content, elliptical and rounded pores with thicker walls were observed in the samples grown at 5% H<sub>2</sub>O and 10% H<sub>2</sub>O content. Moreover, while the tube formations were part of a continuous oxide layer in the samples prepared at 2.5% and 5% H<sub>2</sub>O contents, they were much more distinct and separated from each other in the sample prepared at 10% H<sub>2</sub>O. These differences, as well as the mixed crystalline phases which were described in XRD analyzes affected the capacitive response of the surface by affecting the dielectric constant and the overall surface area of the oxide. Also, the parameter *n*, which could be considered as an indicator of deviation from a perfect capacitive response for *Y*<sub>0</sub>. In this respect, the value *n* ranged from 0 to 1, where 1 described a perfect capacitor [44]. Specifically in electrochemistry and impedance spectroscopy, this value could be evaluated as a measure of roughness [3]. Surfaces with *n*<0.8 were generally accepted as rough surfaces. In our case, as could be followed in Table 3, *n*<sub>w</sub> values increased with respect to H<sub>2</sub>O content in anodizing solution. According to Figure 3, the lowest *n* value, which was observed for 2.5% H<sub>2</sub>O content, had the thinnest pore edges and clearly the roughest surface among other samples.

**Table 3.** Equivalent electrical circuit fitting results of anodized Ti6Al4V samples.

H <sub>2</sub> O percentage	R <sub>sol</sub> (ohm)	R <sub>br</sub> (ohm) x10 <sup>3</sup>	C <sub>br</sub> (F) x10 <sup>-6</sup>	Y <sub>0w</sub> (S.s <sup>n</sup> ) x10 <sup>-5</sup>	n <sub>w</sub>	R <sub>w</sub> (ohm) x10 <sup>3</sup>	C <sub>w</sub> (F) x10 <sup>-6</sup>	Y <sub>0pr</sub> (S.s <sup>n</sup> ) x10 <sup>-5</sup>	n <sub>pr</sub>	R <sub>pr</sub> (ohm) x10 <sup>3</sup>	C <sub>pr</sub> (F) x10 <sup>-6</sup>
2.5	6.08	132	156	2.66	0.8	557	60.7	1.23	1.0	120	12.3
5	11.5	9.85	107	8.10	0.7	127	216	2.06	1.0	247	20.6
10	57.1	27	426	1.99	1.0	17.3	19.9	6.95	0.8	162	130

R<sub>pr</sub> and C<sub>pr</sub> values were used to describe the pore structure of the anodized samples. In this respect, although R<sub>pr</sub> values were similar, C<sub>pr</sub> values increased with increasing H<sub>2</sub>O content in the anodizing solution. The highest C<sub>pr</sub> value of 130 μF was observed on the sample anodized at 10% H<sub>2</sub>O content. This finding was a good indicator of pore structure. Although no significant change in pore diameter was observed, the increase in capacitive response could be explained by the fact that the electrochemical response in the pores became more difficult. Frequency dependent response of a solid-state capacitor and the capacitive behavior in a solution in electrochemistry shared common ground, they posed a very different meaning in terms of material properties. From this point of view, capacitive response of a solid-state capacitor depended solely on the dielectric constant of the material in this structure [3,44]. However, in a solution, the capacitive response was affected by the ions, the transfer of ions in the solution and the oxide structure [28,45]. It should be noted that capillary effect of the tubes and high viscosity of the EG were also important factors for the observed high capacitive values [43,46].

In our analyzes, R<sub>br</sub> and C<sub>br</sub> values indicated the properties of the barrier layer of TiO<sub>2</sub>. In this respect, the barrier layer of the native oxide film, C<sub>ox</sub> and the barrier layer of the nanotubes might be comparable. The C<sub>ox</sub> value of Ti6Al4V and the C<sub>br</sub> values of anodized samples showed good agreement. According to physical definition of a capacitor, the thickness of the oxide layer in impedance spectroscopy could be calculated and it was inversely proportional to the value of the C<sub>br</sub> [47]. Thus, it

could be assumed that the thickness values of the barrier layers were similar. It should also be noted that the highest barrier/oxide film capacitance was calculated as 426  $\mu\text{F}$  on the sample prepared at 10%  $\text{H}_2\text{O}$ . Noting that 10%  $\text{H}_2\text{O}$  content was the highest  $\text{H}_2\text{O}$  content in this study, the results indicated that the sample that was prepared at 10%  $\text{H}_2\text{O}$  content had the thinnest barrier oxide. It was also interesting that, as can be seen in Figure 4 and Figure 5, the sample prepared at 10%  $\text{H}_2\text{O}$  content had the thinnest barrier oxide among all samples, including the native oxide of Ti6Al4V, but had significantly better corrosion properties than the native oxide film.

#### 4. CONCLUSIONS

This study was carried out to observe the formation of  $\text{TiO}_2$  nanotubes on the Ti6Al4V substrate in  $\text{NH}_4\text{F}$  containing EG solution with different  $\text{H}_2\text{O}$  contents and to compare the corrosion and electrochemical behavior of the  $\text{TiO}_2$  nanotubes and the native oxide on Ti6Al4V substrate. Considering that the  $\text{H}_2\text{O}$  content also changes the  $\text{F}^-$  ion concentration in the anodizing medium, their combined effects resulted in some notable differences in both the crystal structure and physical properties of the nanotubes.

According to our findings, regardless of  $\text{H}_2\text{O}$  content in anodization medium, all anodized samples exhibited crystalline structures consisted of rutile and anatase. However, the highest crystallinity was observed on the sample anodized at 5%  $\text{H}_2\text{O}$  content. According to the FESEM images, a correlation between the crystalline structure and the physical structure of the nanotubes was obtained. For the sample prepared at 5%  $\text{H}_2\text{O}$  content, round pores with well-defined tubular structure in a continuous single oxide layer was found. At higher  $\text{H}_2\text{O}$  contents; singular, distinct and well-formed nanotube structures were observed and the thickness of the nanotube layer decreased with the increasing  $\text{H}_2\text{O}$  content in anodizing medium. Both potentiodynamic polarization and EIS analyses revealed that all anodized samples showed better corrosion behavior than untreated Ti6Al4V in Ringer's solution. The electrical equivalent circuit fits obtained from EIS, showed that the capacitive behavior of the tube wall decreased with increasing  $\text{H}_2\text{O}$  content in the anodization solution.

In conclusion, anodized samples with  $\text{TiO}_2$  nanotubes on their surfaces were more beneficial in terms of corrosion resistance in Ringer's solution than untreated Ti6Al4V, and the increase in  $\text{H}_2\text{O}$  content in the anodizing medium affected the structure and morphology of the obtained nanotubes and caused a decrease in corrosion resistance.

#### ACKNOWLEDGEMENTS

This study was supported by Yildiz Technical University, Scientific Research Projects Coordinations (YTU BAPK) with the project number FDK2018-3744.

#### References

1. A. Yamagami, N. Nagaoka, K. Yoshihara, M. Nakamura, H. Shirai, T. Matsumoto, K. Suzuki, Y. Yoshida, *Dent. Mater. J.*, 33 (2014) 828.
2. J. Yang, H. Zhang, S. Man Chan, R. Li, Y. Wu, M. Cai, A. Wang, Y. Wang, *Int. J. Nanomed.* 15

- (2020) 3523.
3. W.Q. Yu, J. Qiu, L. Xu, F.Q. Zhang, *Biomed. Mater.*, 4 (2009) 065012.
  4. L. v. Taveira, J.M. Macák, H. Tsuchiya, L.F.P. Dick, P. Schmuki, *J. Electrochem. Soc.*, 152 (2005) B405.
  5. L. Wermuth, M. Kolb, T. Mertens, T. Strobl, D. Raps, *Prog. Org. Coat.*, 87 (2015) 242.
  6. I. Roman, R.D. Trusca, M.L. Soare, C. Fratila, E. Krasicka-Cydzik, M.S. Stan, A. Dinischiotu, *Mater. Sci. Eng., C*, 37 (2014) 374.
  7. G. Wang, S. Moya, Z. Lu, D. Gregurec, H. Zreiqat, *Nanomedicine*, 10 (2015) 1327.
  8. W.T. Kim, W.Y. Choi, *J. Nanomaterials*, 2019 (2019) 1.
  9. D. Regonini, *Mater. Sci. Eng., R*, 74 (2013) 377.
  10. O. Robinson Aguirre, E. Félix Echeverría, *Appl. Surf. Sci.*, 445 (2018) 308.
  11. Q. Wang, Y. Zhang, K.E. Yang, L. Tan, *Surf. Rev. Lett.*, 16 (2009) 775.
  12. D. Regonini, A. Satka, A. Jaroenworarluck, D.W.E. Allsopp, C.R. Bowen, R. Stevens, *Electrochim. Acta*, 74 (2012) 244.
  13. D.G. Li, D.R. Chen, J.D. Wang, P. Liang, *Electrochim. Acta*, 207 (2016) 152.
  14. J.S. Khaw, C.R. Bowen, S.H. Cartmell, *Nanomaterials*, 10 (2020) 1.
  15. D.J. Hall, R.M. Urban, R. Pourzal, T.M. Turner, A.K. Skipor, J.J. Jacobs, *J Biomed Mater Res B Appl Biomater.*, 105 (2017) 283.
  16. S. Li, M. Zhu, J. Liu, M. Yu, L. Wu, J. Zhang, H. Liang, *Appl. Surf. Sci.*, 316 (2014) 28.
  17. F.S. Utku, E. Yuca, E. Seckin, G. Goller, A.Y. Karatas, M. Urgan, C. Tamerler, *Bioinspired Biomimetic Nanobiomater.*, 4 (2015) 155.
  18. G. Strnad, Z. German-Sallo, L. Jakab-Farkas, R. Cazacu, D. Portan, *Procedia Manuf.*, (2018) 19.
  19. S. Poddar, A. Bit, S.K. Sinha, *Mater. Chem. Phys.*, 254 (2020) 123457.
  20. S. Saha, R. Kumar, K. Pramanik, A. Biswas, *Appl. Surf. Sci.*, 449 (2018) 152.
  21. A. Radtke, A. Topolski, T. Jędrzejewski, W. Kozak, B. Sadowska, M. Więckowska-Szakiel, M. Szubka, E. Talik, L.P. Nielsen, P. Piszczek, *Nanomaterials*, 7 (2017) 197.
  22. Z.J. Liu, X. Zhong, H. Liu, I.L. Tsai, U. Donatus, G.E. Thompson, *Electrochim. Acta*, 182 (2015) 482.
  23. V. Sivaprakash, R. Narayanan, *J. Bio- Tribo-Corros.*, 6:105 (2020) 1.
  24. Z. Su, L. Zhang, F. Jiang, M. Hong, *Prog. Nat. Sci.: Mater. Int.*, 23 (2013) 294.
  25. Y. Fu, A. Mo, *Nanoscale Res. Lett.*, 13 (2018) 187.
  26. Y. Liu, D. Yu, Y. Song, D. Li, S. Zhang, W. Ma, Z. Wei, X. Zhu, *J. Solid State Electrochem.*, 19 (2015) 1403.
  27. H.M. Mateus, J. Bautista-Ruiz, J. Barba-Ortega, M.R. Joya, *Rasayan J. Chem.*, 12 (2019) 1304.
  28. K. Indira, U.K. Mudali, T. Nishimura, N. Rajendran, *J. Bio- Tribo-Corros.*, 1:28 (2015) 1.
  29. Y. Wang, D. Yu, B. Chong, D. Li, Y. Song, S. Zhang, W. Ma, X. Zhu, *J. Electrochem. Soc.*, (2014) H89.
  30. N.J. Suliali, C.M. Mbulanga, W.E. Goosen, J.R. Botha, *Mater. Sci. Semicond. Process.*, 109 (2020) 104931.
  31. J.M. Macak, H. Tsuchiya, L. Taveira, S. Aldabergerova, P. Schmuki, *Angew. Chem. Int. Ed.*, 44 (2005) 7463.
  32. Powder Diffraction File, Joint Committee on Powder Diffraction Standards (JCPDS), ASTM, 2003, Card number: 65-4920.
  33. Powder Diffraction File, Joint Committee on Powder Diffraction Standards (JCPDS), ASTM, 2003, Card number: 89-4921.
  34. Powder Diffraction File, Joint Committee on Powder Diffraction Standards (JCPDS), ASTM, 2003, Card number: 89-4746.
  35. H. Tsuchiya, J.M. Macak, A. Ghlcov, P. Schmuki, *Small*, 2 (2006) 888.
  36. B. Yang, M. Uchida, H.M. Kim, X. Zhang, T. Kokubo, *Biomater.*, 25 (2004) 1003.
  37. V.S. Saji, H.C. Choe, W.A. Brantley, *Acta Biomater.*, 5 (2009) 2303.

38. E. Filova, J. Fojt, M. Kryslova, H. Moravec, L. Joska, L. Bacakova, *Int. J. Nanomed.*, 10 (2015) 7145.
39. A. Valota, D.J. LeClere, P. Skeldon, M. Curioni, T. Hashimoto, S. Berger, J. Kunze, P. Schmuki, G.E. Thompson, *Electrochim. Acta*, 54 (2009) 4321.
40. I.M. Pohrelyuk, V.M. Fedirko, O. v. Tkachuk, R. v. Proskurnyak, *Corros. Sci.*, 66 (2013) 392.
41. M. Luqman, A.H. Seikh, A. Sarkar, S.A. Ragab, J.A. Mohammed, M.F. Ijaz, H.S. Abdo, *Crystals*, 10 (2020) 190.
42. M. Tertiş, A. Florea, B. Feier, I.O. Marian, L. Silaghi-Dumitrescu, A. Cristea, R. Săndulescu, C. Cristea, *J. Nanosci. Nanotechnol.*, 15 (2015) 3385.
43. A. Bervian, E. Coser, S. Khan, S.A. Pianaro, C. Aguzzoli, J.S. Marcuzzo, M.R. Baldan, C. de Fraga Malfatti, *Mater. Res.*, 20 (2017) 962.
44. C. Liu, Q. Bi, A. Leyland, A. Matthews, *Corros. Sci.*, 45 (2003) 1243.
45. T.F. Otero, J.G. Martinez, K. Asaka, *Front. Mater.*, 3 (2016) 3.
46. G. Liu, K. Du, K. Wang, *Appl. Surf. Sci.*, 388 (2016) 313.
47. B. Hirschorn, M.E. Orazem, B. Tribollet, V. Vivier, I. Frateur, M. Musiani, *Electrochim. Acta*, 55 (2010) 6218.

© 2022 The Authors. Published by ESG ([www.electrochemsci.org](http://www.electrochemsci.org)). This article is an open access article distributed under the terms and conditions of the Creative Commons Attribution license (<http://creativecommons.org/licenses/by/4.0/>).